LAVA FLOWS IN MARE IMBRIUM: AN EVALUATION OF ANOMALOUSLY LOW EARTH-BASED RADAR REFLECTIVITY

GERALD G. SCHABER
U.S. Geological Survey, Flagstaff, Ariz., U.S.A.

THOMAS W. THOMPSON
Jet Propulsion Laboratory, Pasadena, Calif., U.S.A.

and

STANLEY H. ZISK
Massachusetts Institute of Technology, Haystack Observatory, Westford, Mass., U.S.A.

(Received 13 March, 1975)

Abstract. The lunar maria reflect two to five times less Earth-based radar power than the highlands, the spectrally blue maria surfaces returning the lowest power levels. This effect of weakening signal return has been attributed to increased signal absorption related to the electrical and magnetic characteristics of the mineral ilmenite ($FeTiO_3$).

The surface of Mare Imbrium contains some of the most distinct red-blue colorimetric boundaries and depolarized 70 cm wavelength reflectivity variations on the near side of the Moon. The weakest levels of both 3.8 cm and 70 cm reflectivity within Imbrium are confined to regional mare surfaces of the blue spectral type that can be recognized as stratigraphically unique flow surfaces. Frequency distributions of the 70 cm polarized and depolarized radar return power for five mare surfaces within the basin indicate that signal absorption, and probably the ilmenite content, increases generally from the beginning of the Imbrian Period to the end of the Eratosthenian Period with slight reversal between the end of the Imbrian and beginning of the Eratosthenian.

TiO_2 calibrated radar reflectivity curves can be utilized for lunar maria geochemical mapping in the same manner as the TiO_2 calibrated spectral reflectivity curves of Charette *et al.* (1974). The long wavelength radar data may be a sensitive indicator of mare chemical variations as it is unaffected by the normal surface rock clutter that includes ray materials from large impact craters.

1. Introduction

The surface of Mare Imbrium contains some of the most distinct 'red-blue' colorimetric boundaries and depolarized 70 cm radar backscatter variations on the near side of the Moon. Obtained at greatly diverse electromagnetic frequencies, a surprisingly good correlation exists between these two data sets. In the present investigation we integrate detailed stratigraphic information for the Imbrium basin with available radar and color data in order to establish the physical and/or chemical relations between distinct mare surfaces, radar reflectivity, and spectral color data.

A number of the color boundaries within Imbrium were shown by Strom (Kuiper, 1965; Whitaker, 1972) to correlate with the scarps of relatively young lava flows recently mapped in detail by Schaber (1973). The association of these lava flows with weak depolarized radar return at 70 cm had been demonstrated (Schaber *et al.*, 1972).

The radar data were produced by transmitting circularly polarized radiation and by analyzing the returned signal into (1) a component polarized opposite to that of

The Moon **13** (1975) 395–423.

the original pulse, and (2) a component with polarization the same as that of the original pulse. The first is called the 'polarized' signal, since it has the polarization expected from a specular reflector (perfectly smooth sphere), the second component the 'depolarized' signal, which is orthogonal to the polarized component. A detailed account of the doppler-delay radar mapping technique can be found in Pettingill *et al.* (1974), Thompson and Zisk (1972), and Zisk *et al.* (1974).

Two distinct physical processes are responsible for the observed echoes (Rea *et al.*, 1964; Hagfors, 1967; Pettengill *et al.*, 1974). In the first, called quasi-specular reflection, the echoes are highly polarized and show a sharp decrease of power with increase in angle of incidence. The major portion of the radar echo is of this type, and it has been attributed to scattering from a large number of smooth facets, many wavelengths in size, oriented normal to the radar signal (Brown, 1960). The second process, diffuse scattering, accounts for all of the polarized echoes and most polarized echoes beyond angles of incidence of 40 deg. Diffuse scattering is generally thought to be caused by single or multiple scattering of radar echoes by rocks on the surface and/or within the upper few meters of the regolith (Hagfors, 1967; Burns, 1969; Thompson and Zisk, 1972; Pollack and Whitehill, 1972).

Thompson *et al.* (1974) have shown that greatly enhanced depolarized 3.8 cm and 70-cm radar signals can be correlated with the increased roughness of fresh impact craters (crater walls and blocky ejecta). We suggest here that weaker-than-normal mare backscatter is caused by an entirely different process involving increased signal absorption within the regolith, this being related to the effect of ilmenite ($FeTiO_3$) on increasing electrical and magnetic losses in the material.

We agree with Pollack and Whitehill (1972) that the observed 1:2 minimum difference in returned depolarized power from the lunar mare and highlands, respectively, is a measure of the absorption properties of the surface materials and is probably caused by increasing concentrations of ilmenite from gabbroic-anorthosite (highlands) to titaniferous basalt (maria) materials. Evidence is presented to show that the real, but little understood, effect of Ti–Fe chemistry on the radar absorption is so sensitive that distinct, intramare surfaces mapped within Mare Imbrium can be clearly delineated by analysis on the frequency distribution of returned radar power.

2. Radar Reflectivity in Mare Imbrium

The areas of weakest * 70 cm polarized and depolarized backscatter in Mare Imbrium all fall on spectrally blue mare surfaces of both Imbrian and Eratosthenian age. Three eruptive phases of volcanism in the Eratosthenian, designated from oldest to youngest phase I, II, and III were recognized by Schaber (1973) (Figure 1a). Although the weak return areas on the polarized map are discontinuous and less discrete than on the

* The backscatter levels indicated in Figures 1b, c, are $> 50\,\%$ down in power from the average blue mare characteristic of the west side of the basin and $> 75\,\%$ down in power from the average red mare of Imbrian age that occupies much of the eastern half of the basin. The above levels of backscatter will hereafter be referred to as weak return for convenience.

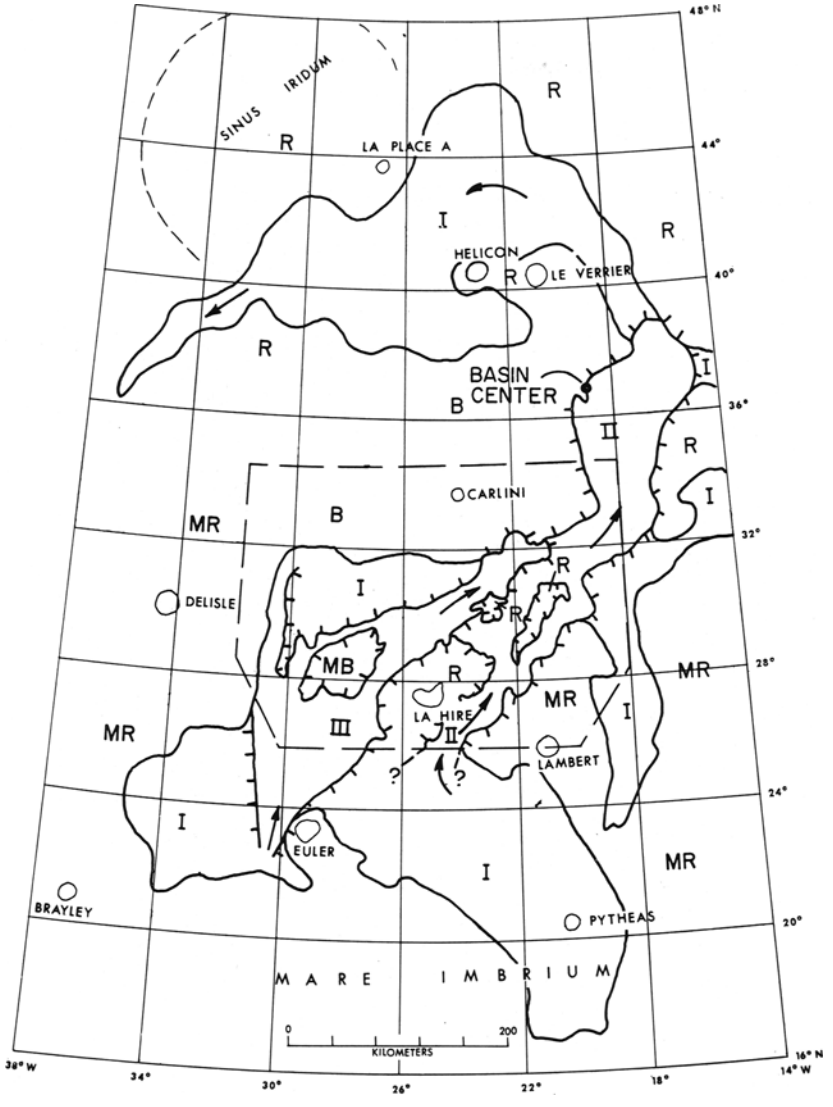

Fig. 1a. Part of Mare Imbrium, showing distribution of Eratosthenian and Imbrian mare surfaces (Wilhelms and McCauley, 1971; Schaber, 1973). Eratosthenian surfaces shown within solid outlines are designated from oldest to youngest phase I, II, or III. Lines with hachures indicate maximum extent of phase II and III lava flow scarps described by Schaber (1973). All Eratosthenian mare surfaces are of the blue spectral type. Colorimetric properties of Imbrian surfaces shown by B (blue), MB (medium blue), MR (medium red) and R (red). Color data taken from composite UV-IR photograph (see Figure 2). Arrows indicate direction of lava flow movement. Dashed area outlines area of photograph and sketch maps of Figures 5a, b, c discussed in text.

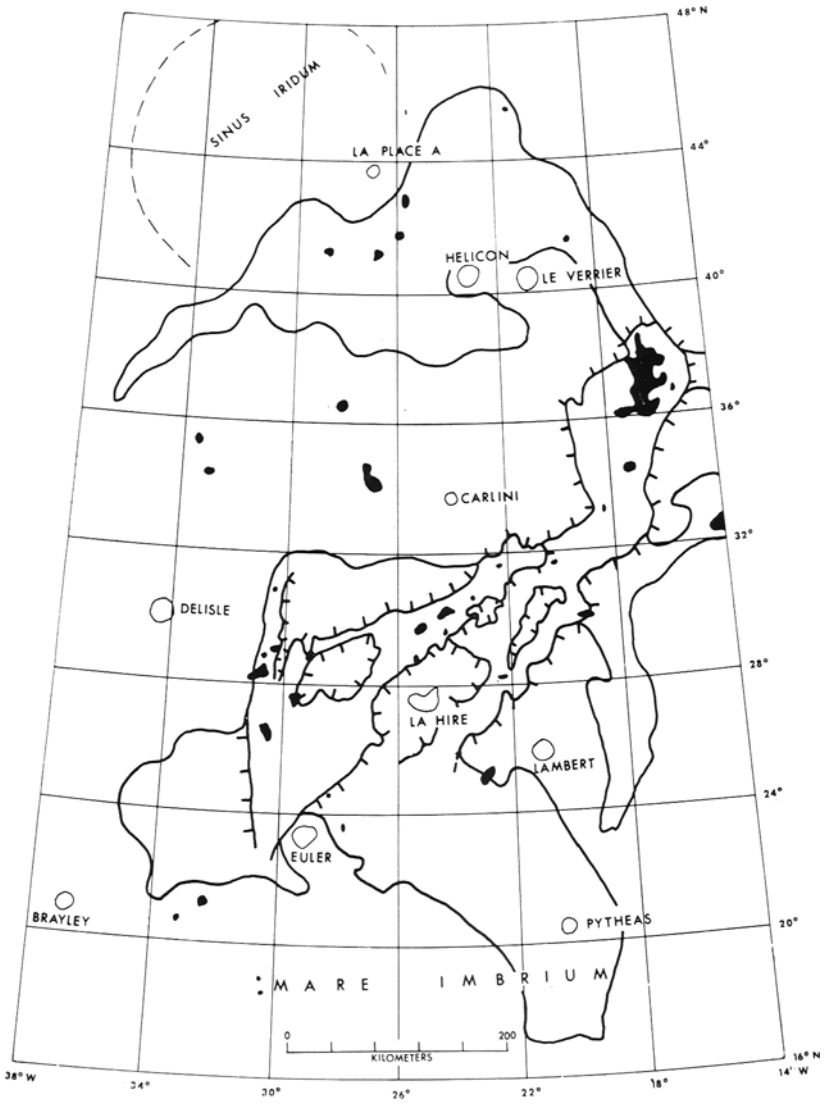

Fig. 1b. Part of Mare Imbrium showing the distribution of polarized 70 cm radar return with less than 50 % average power for the basin (black areas). (See Figure 1a caption for colorimetric information, description of mapped areas, and symbols.)

depolarized map, the correlation between low radar return and blue mare is obvious on both maps. We can assume that the weakest returns on the polarized map can be chiefly attributed to a local decrease in the parameters responsible for diffuse scattering, as the reduction in signal is even more marked on the depolarized map (Pettengill and Thompson, 1968; Thompson and Zisk, 1972; Thompson, 1974).

By comparing the schematic radar maps (Figures 1b, 1c) with a black and white

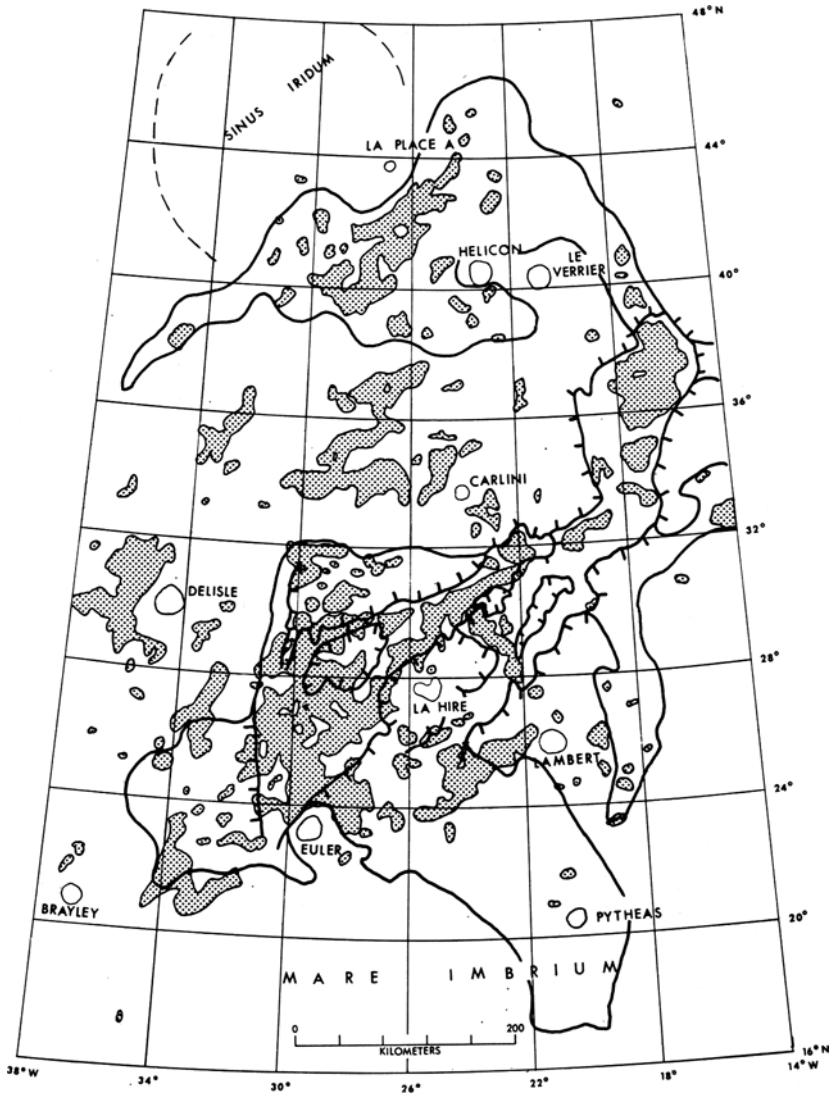

Fig. 1c. Part of Mare Imbrium showing distribution (stippled areas) of depolarized 70 cm radar return with less than 50 % average power for the basin. Note excellent agreement of weak radar return from phase III flows (Figure 1a). Description of mapped areas and other symbols same as Figure 1a.

print of an ultraviolet-infrared color composite photograph* of the Mare Imbrium region (Figure 2) a correlation can be seen to exist between the below-average levels of 70-cm depolarized backscatter and the blue mare surfaces of both Imbrian and Eratosthenian age. On the UV-IR composite photograph, however, none of the

* By courtesy of Ewen Whitaker (Lunar and Planetary Laboratory, University of Arizona, Tucson, Ariz., U.S.A.).

separately mapped blue mare surfaces shown on Figure 1a can be delineated where they are in contact with one another. The rather poor separation of the blue mare surfaces on the UV-IR map (Figure 2) is seen in Figures 3a, b, which show the relative blue-red spectral reflectivity of two Imbrian and three Eratosthenian surfaces scanned (Figure 4) from a digitized version of the Figure 2 photograph. Note that blue mare surfaces of both the Imbrian and Eratosthenian age have about the same relative blueness, whereas the Imbrian red surface is shifted considerably to the red. The slight increase in redness shown by the Eratosthenian phase III is thought to be an effect of abundant aluminum-rich Copernicus ray materials in southern Mare

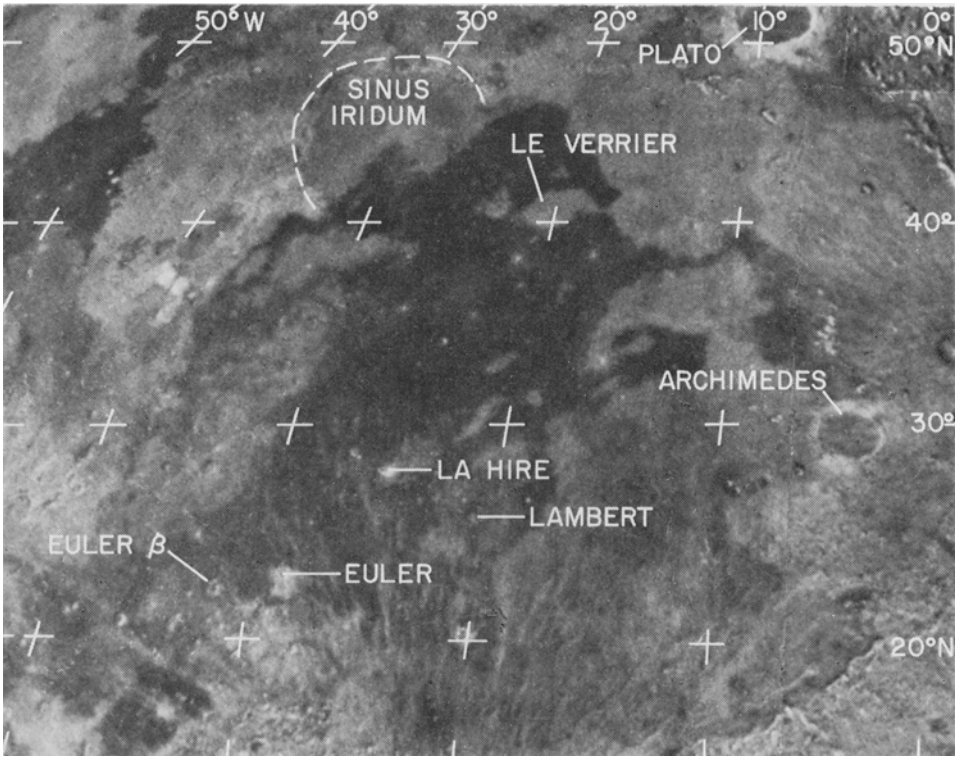

Fig. 2. Black and white version of a composite infrared and ultraviolet photograph showing distribution of red (light tones) and blue (dark tones) mare surfaces within Mare Imbrium. Photograph courtesy of Ewen Whitaker (Lunar and Planetary Laboratory, University of Arizona). Compare with Figure 1c.

Imbrium. The distribution of weak-return levels of depolarized radar power thus appears to be a better discriminator of these mappable flow surfaces than the currently available colorimetric photography. A new set of higher resolution red-blue color maps will soon be available and these might prove to be better discriminators of the individual blue flows (Whitaker, 1974).

The agreement of 70-cm polarized and depolarized weak return with geologically mapped flow units is best seen in the region of the youngest Eratosthenian eruptives shown in Figures 5a, b, c and indexed in Figure 1a. It is clear that a large concentration of depolarized weak return data lies within the boundaries of the phase III lavas as the youngest eruptives in the basin. The depolarized weak-return data represented by 'A' (Figure 5c) closely follows the most extensive (400 km) flow of that eruptive sequence. A significant number of the smaller, isolated, weak return areas correlate with blue phase II surfaces, others are associated with blue materials of Imbrian age. Note how both the polarized and depolarized weak return data are absent from the red mare patches (labeled 'R').

The distribution of depolarized weak-return data at the 3.8 cm wavelength (Figure 6), though spotty due to the nature of surface backscatter at this shorter wavelength, does follow closely the distribution observed at 70 cm. The distribution of weak return

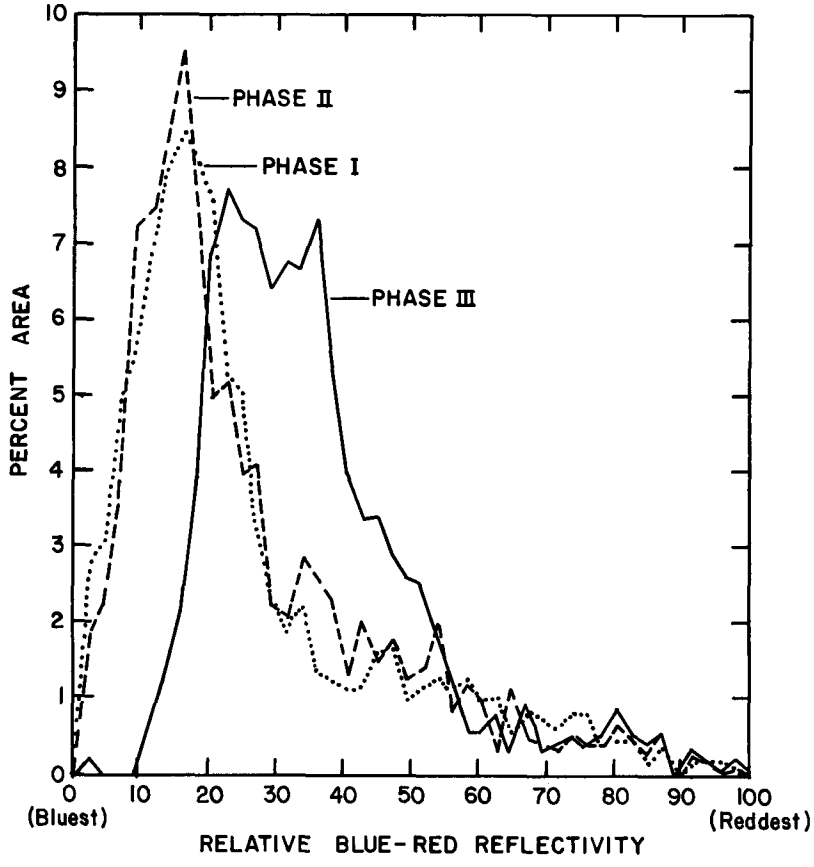

Fig. 3a. Surface-area distribution of relative blue-red spectral reflectivity for the Eratosthenian (phase I, II, and III) surfaces within Mare Imbrium. Areas scanned (Figure 4) from a digitized version of the UV-IR color map (Figure 2). The bluest (0) and reddest (100) values represent the highest and lowest film density values measured within each area.

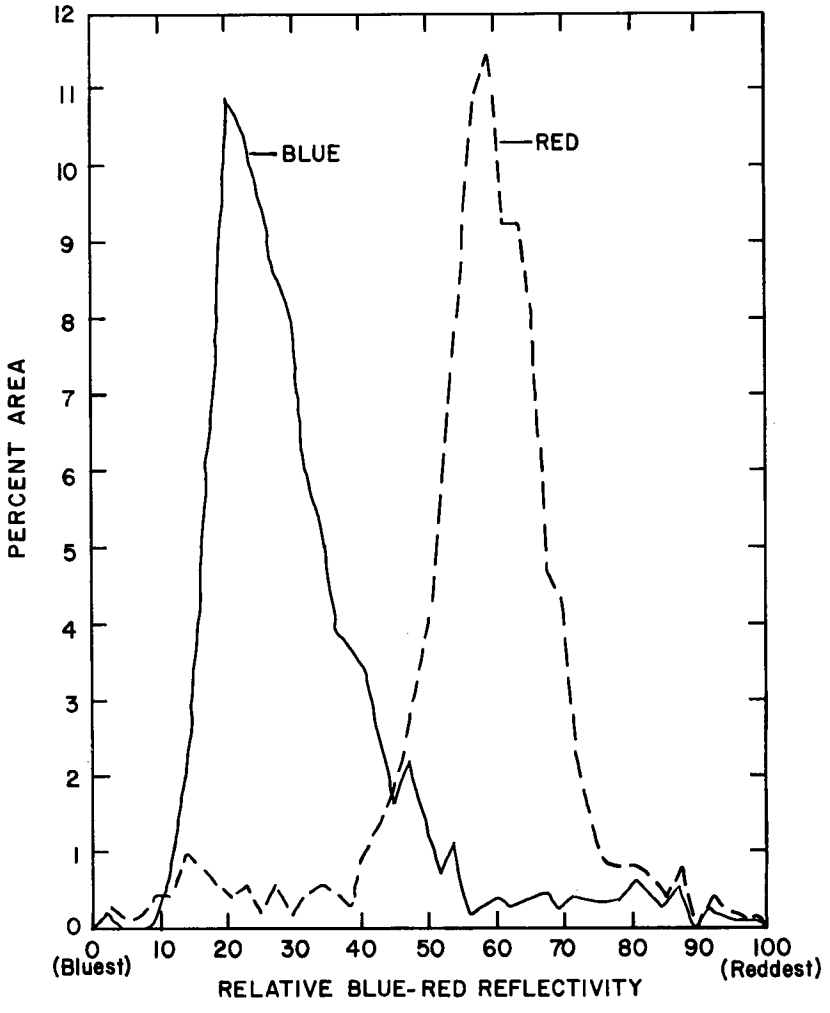

Fig. 3b. Surface-area distribution of relative blue-red spectral reflectivity for the Imbrian red and blue mare surfaces within Mare Imbrium. Areas scanned shown in Figure 4. See caption of Figure 3a for explanation.

tends to concentrate on the youngest (phase III) blue lavas of Eratosthenian age and are clearly absent from the underlying red mare surfaces. The shorter wavelength maps show much more variability since the short wavelengths are more sensitive to background 'noise' caused by higher population of 1- to 10-cm size surface rocks and small, fresh, primary and secondary craters, more visible in the finer resolution 3.8 cm wavelength maps. Ray materials from the young craters Copernicus, Aristarchus, and Aristillus are very distinct in the 3.8 cm maps but are not seen in the 70 cm data.

There is an excellent correlation of the 3.8 cm depolarized weak return data with the small flow labeled 'X' on Figure 6, not well defined on the depolarized 70 cm data (Figure 5c).

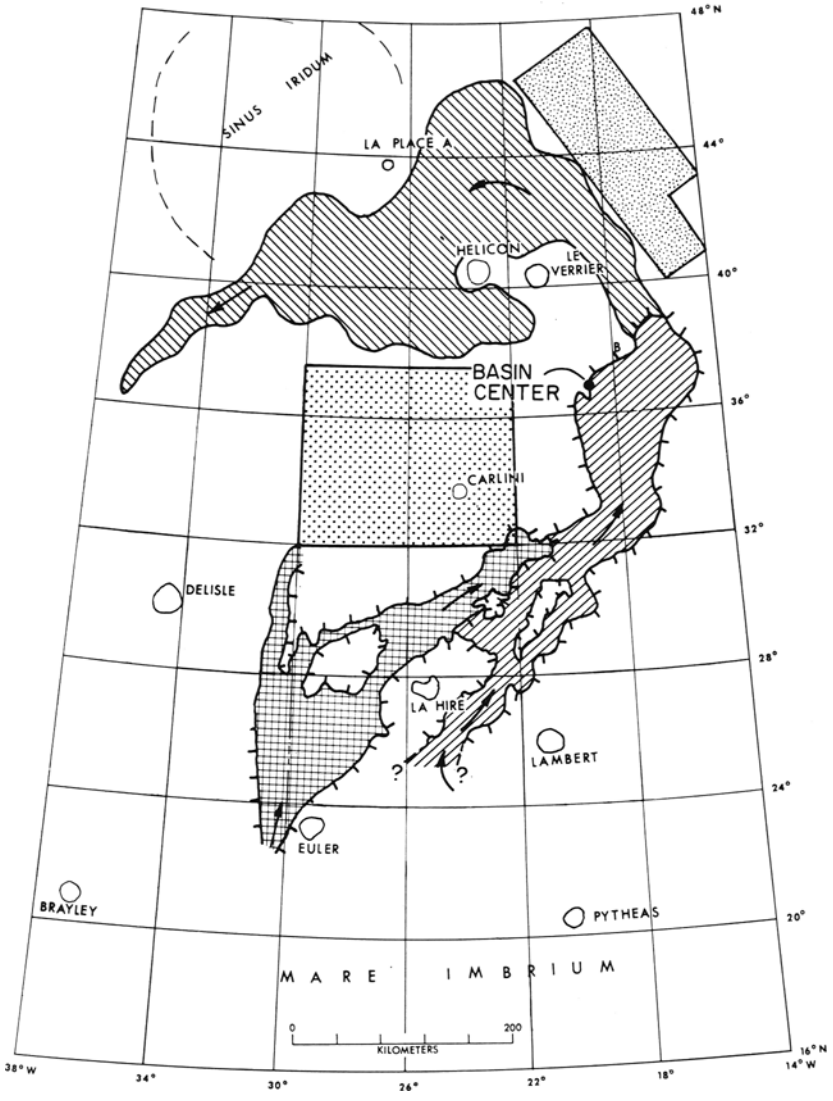

Fig. 4. Areas within Mare Imbrium used to generate the data presented in Figures 3a and b, and Figures 7a, b, and c. Small stipple, Imbrian red surface; large stipple, Imbrian blue surface; left slant symbol, phase I; right slant symbol, phase II; cross hachured, phase III (Figures 1a, b, and c and Figure 2).

Fig. 5a. Photogeologic map of late Eratosthenian lava flows in southwestern Mare Imbrium (after Schaber, 1973). Hachured lines mapped on flow scarps (barbs point downslope). Arrows indicate position of flow channels and flow direction. Solid lines with double triangles, mare ridge crest. Dashed lines with bar and ball indicate fault (ball on downthrown side). Areas labeled 'R' are red mare (discussed in text); all mapped surfaces are blue. Photobase mosaic composed of rectified Apollo 15 oblique metric photographs (1553, 1556, and 1557). (Rectification by the U.S. Army Map and Topographic Command under NASA contract.)

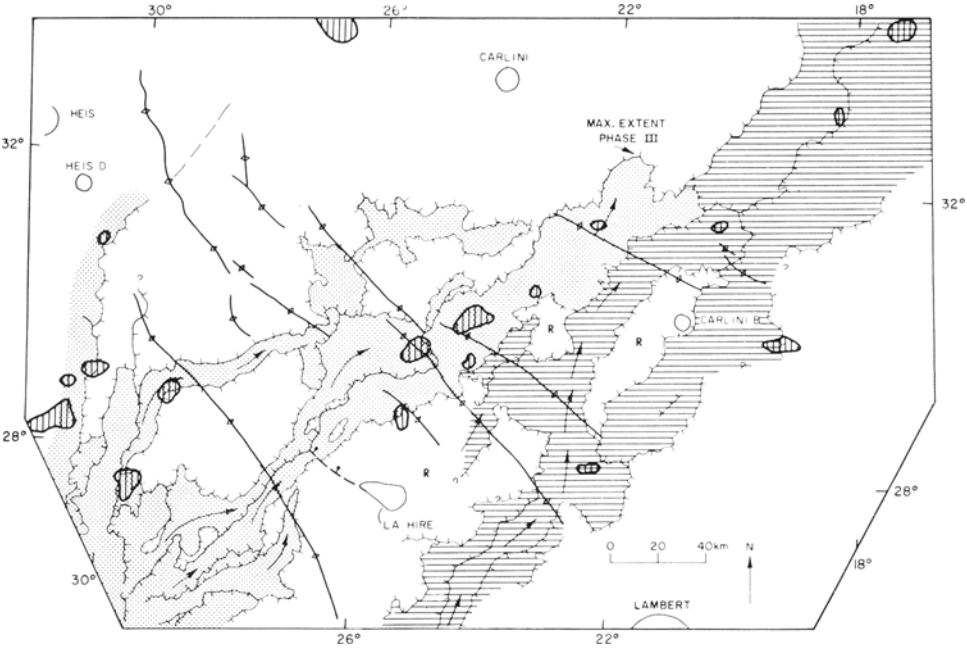

Fig. 5b. Sketch map of Figure 5a photogeologic map showing correlation of weak polarized 70 cm radar return (vertical bars) and Eratosthenian lava eruptives. Phase II flows (cross bars); phase III flows (stippled). See Figure 5a for explanation of other symbols. Radar return shown represents levels less than 50 % of the Imbrium basin average.

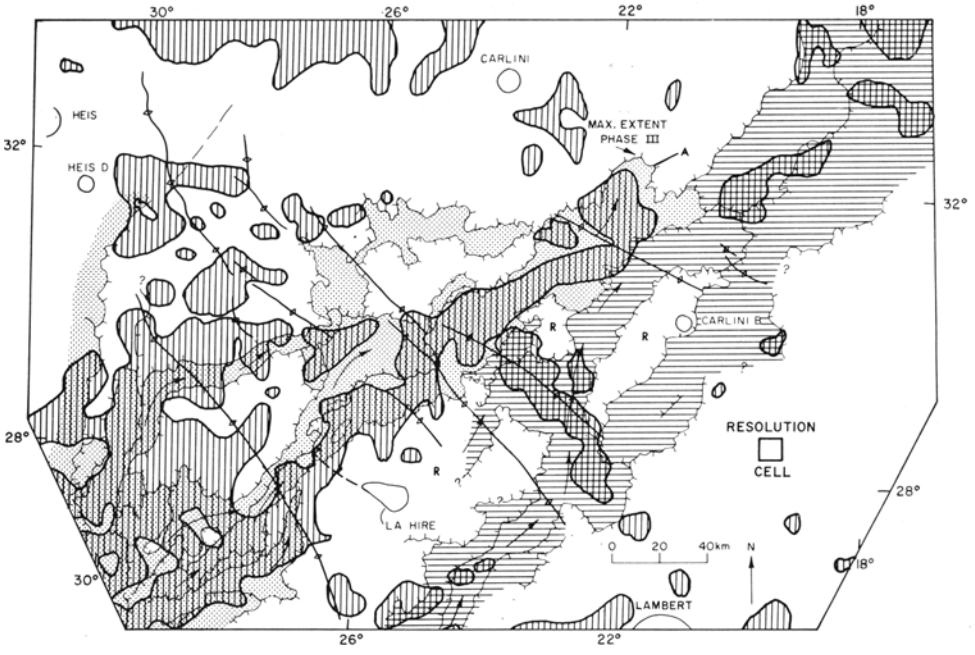

Fig. 5c. Sketch map of Figure 5a photogeologic map showing correlation of weak depolarized 70 cm radar return (vertical bars) and late Eratosthenian lava eruptives. Flow age symbols same as for Figure 5b. Radar return shown represents levels less than 50 % of the Imbrium basin average. 'A' area of depolarized weak return discussed in text.

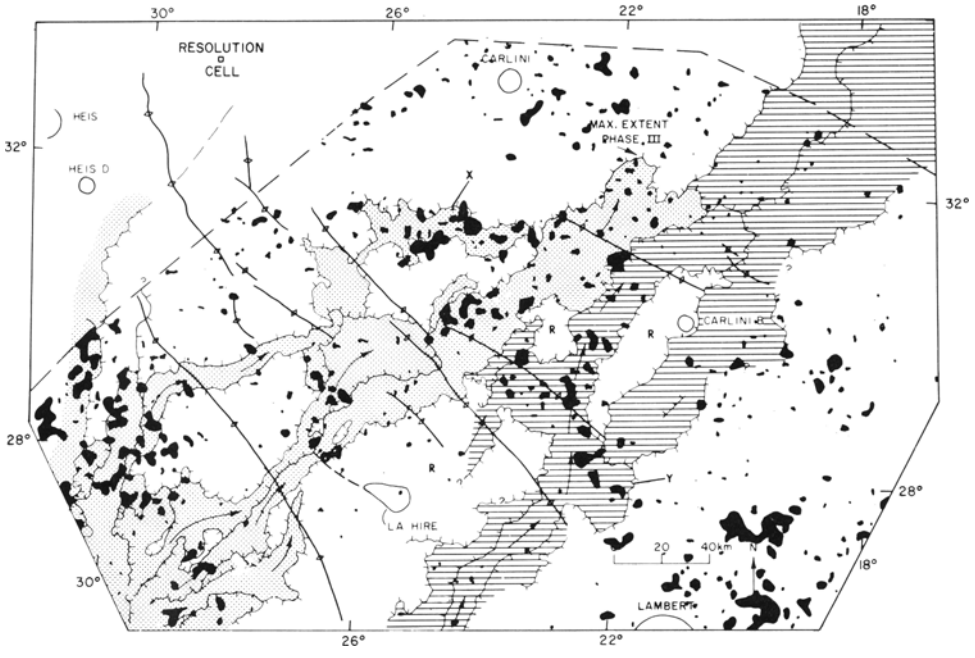

Fig. 6. Sketch map of the Figure 5a photogeologic map showing correlation of weak depolarized 3.8 cm radar return (black areas) and late Eratosthenian lava flows. Flow age and other symbols same as given for Figures 5a, b. 'X' and 'Y' flows showing excellent correlation discussed in text.

3. Radar Power Frequency Distributions

Digital radar images of five distinct Imbrian and Eratosthenian age surfaces within Mare Imbrium (Figure 4) were processed to show areal distributions of polarized and depolarized 70 cm radar power (Figures 7a, b, c). The three Eratosthenian surfaces are of the blue spectral type whereas the oldest Imbrian age surface is extremely red, the youngest quite blue.

The average power decreases with the youth of the surface both in the Imbrian and Eratosthenian Periods as shown by Table I. The young Eratosthenian phase III lava

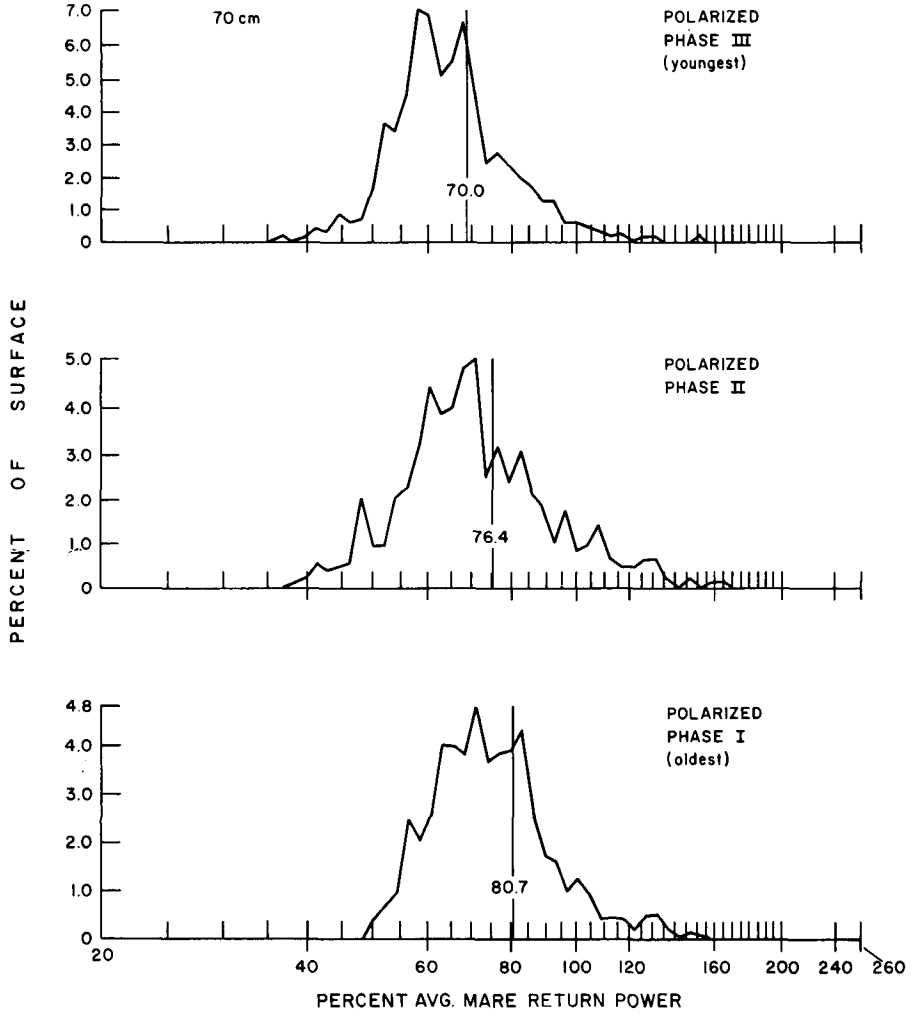

Fig. 7a. Surface area distribution of 70 cm polarized return power for surfaces I, II, and III. Surfaces represented shown in Figure 4. Power levels are given relative to Imbrium basin average of 100. Vertical line (with number) through each peak indicates the average level of power returned from each surface.

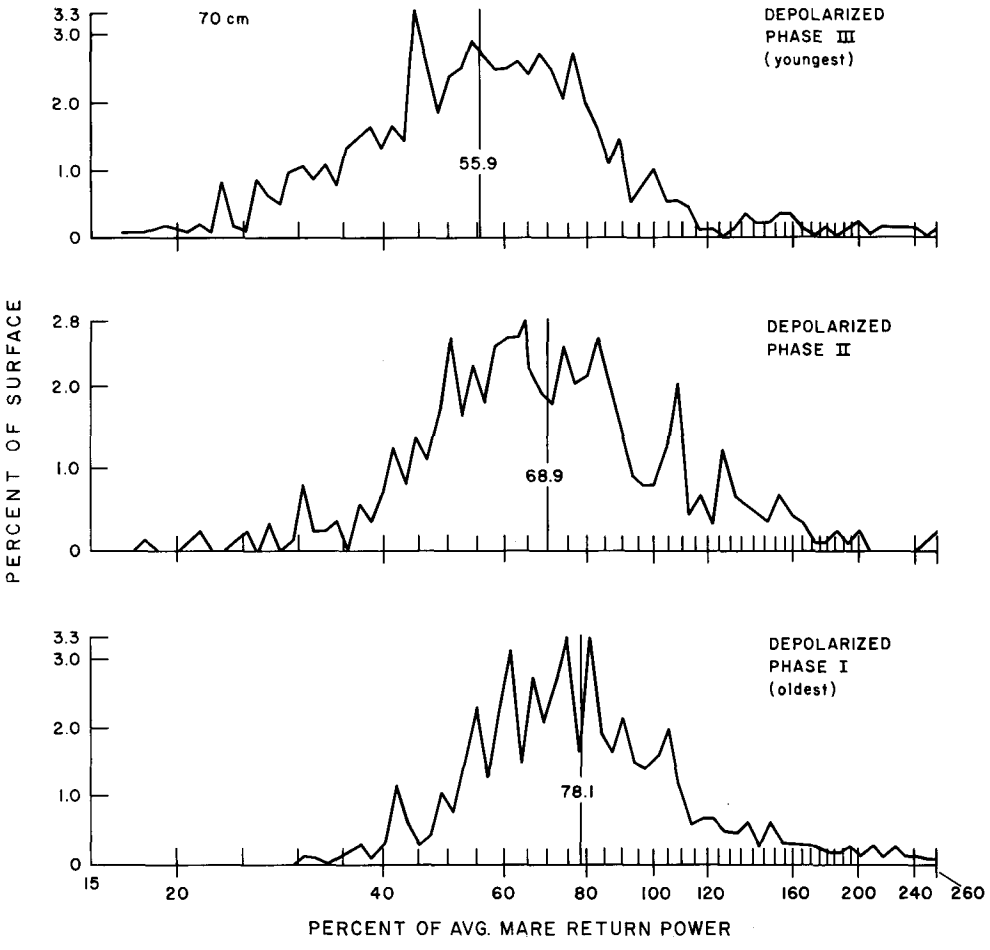

Fig. 7b. Surface area distribution of 70 cm depolarized return power for surfaces I, II, and III. See Figure 7a caption for explanation.

flows, shown earlier to possess the best correlation with lowest levels of 3.8 cm and 70 cm backscatter, are seen on the table to reflect only 56% of the average mare on the depolarized maps and 70% of the average polarized mare return. The Imbrian red mare, on the other hand, reflects one percent more than average polarized return for the basin and 19% more than the average depolarized value for the basin.

The average power return for these surfaces is rather misleading since it is in the low end of the return power scale that the various surfaces appear to be best differentiated. Figure 8 compares the percent of radar return power below the 50% level with cumulative percent of surface area for one Imbrian (Imbrian blue) and three Eratosthenian (phase I, II, and III) blue geologic units. The Imbrian red region (Figure 4) has no return below the 58.5% level and therefore is not included.

The Eratosthenian phase III eruptives, where 40.7% of the surface returns less than

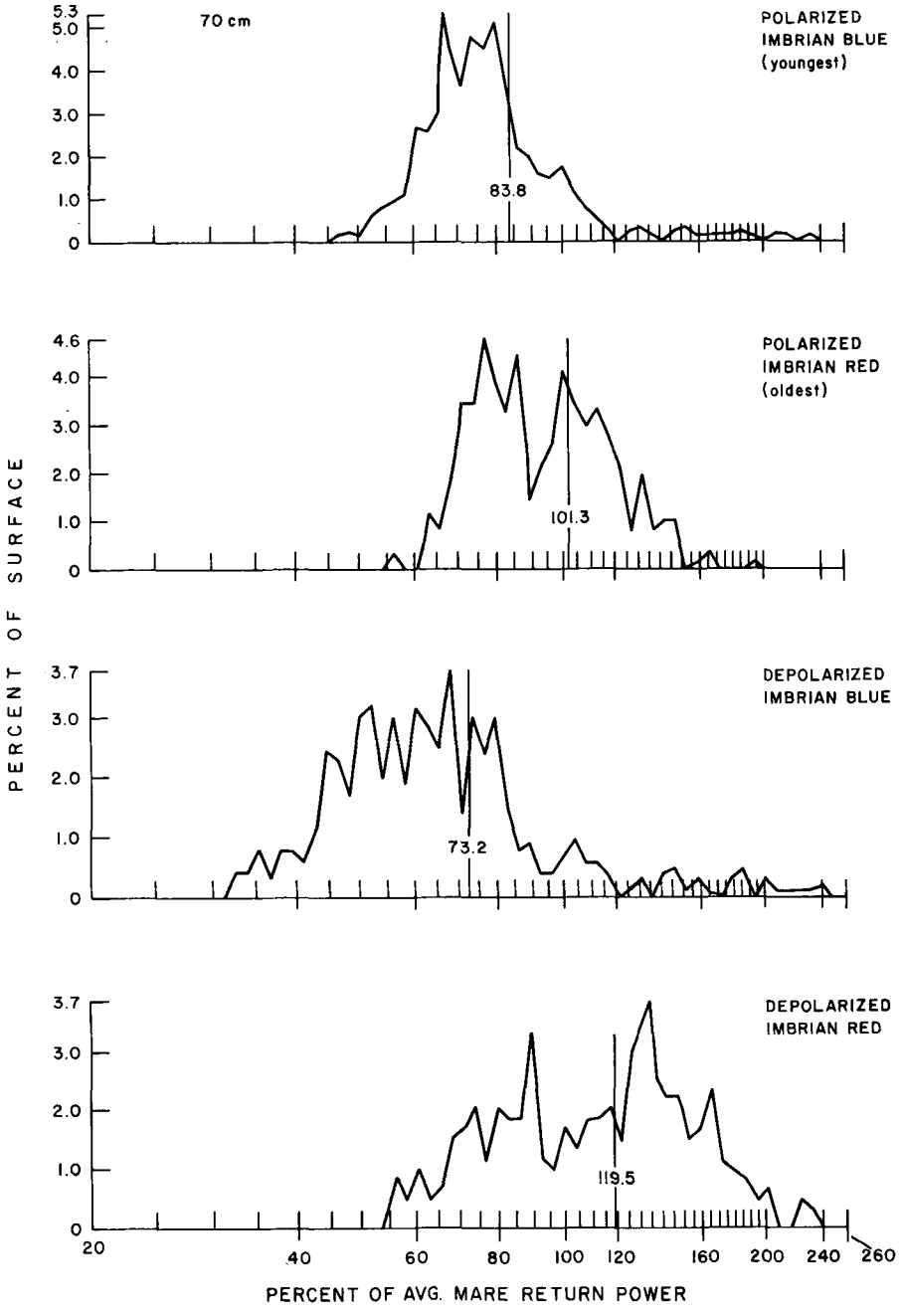

Fig. 7c. Surface area distribution of 70 cm polarized and depolarized return power for surfaces Imbrian blue and Imbrian red. See Figure 7a caption for explanation.

TABLE I

70 cm polarized and depolarized radar statistics for Imbrian and Eratosthenian mare surfaces within Mare Imbrium

Mare unit	Percent of avg. polarized power for basin (avg. = 100)	Standard deviation	Percent of avg. depolarized power for basin (avg. = 100)	Standard deviation	Percent of mare unit area with < 50 % of avg. depolarized power for basin
Eratosthenian					
phase III (youngest)	70.0	10.7	55.9	23.6	40.7
phase II	76.4	14.1	68.9	25.0	23.3
phase I	80.7	11.5	78.1	20.1	9.3
Imbrian					
Imbrian blue	83.8	13.3	73.2	22.1	13.9
Imbrian red (oldest)	101.3	13.0	119.5	18.4	0.0

50% of the average depolarized radar power for the basin, are clearly the poorest radar reflectors; other areas returning less than 50% are phase II, 23.3%, Imbrian blue, 13.9%, and phase I, 9.3% (Table I).

4. Surface and Subsurface Rocks

Differences in the depolarized radar signals have been attributed to variations in the distribution of wavelength size structures, notably rocks, and/or in the ability of the surface layer to absorb the incident radiation and thereby affect the strength of echoes returned from the subsurface (Thompson *et al.*, 1974; Pieters *et al.*, 1973; Pollack and Whitehill, 1972).

Thompson *et al.* (1974) made the assumption that the 3.8 cm radar detects rocks that range in size from 1 cm to 40 cm and are on the surface or buried no deeper than 1 m. Similarly, the 70 cm radar detects those rocks that range from 20 cm to 7 m and are on the surface or buried no deeper than about 20 m. Surveyor television images and Apollo lunar surface photography have confirmed that rocks ranging upward in size from 25 cm are rare. Rocks in the size range effective to the 70 cm radar are generally associated only with ejecta from relatively large (>300 m diam) impact craters that penetrate the regolith. The average cumulative frequency of rocks in the size range 1 cm to 10 m published for various Surveyor and Apollo mare sites reveal that the rock populations on diverse mare surfaces vary little and that an average mare surface contains about 200 times as many 1-cm rocks than 10-cm rocks and 5 times as many 25-cm size boulders as 50-cm boulders (Shoemaker *et al.*, 1968; Shoemaker *et al.*, 1970a, b). The mechanism causing the relatively high average 3.8 cm diffuse backscatter across the Imbrium basin may therefore be partially due to this normally large population of 1–20 cm-sized rock fragments unseen by the 70 cm signals.

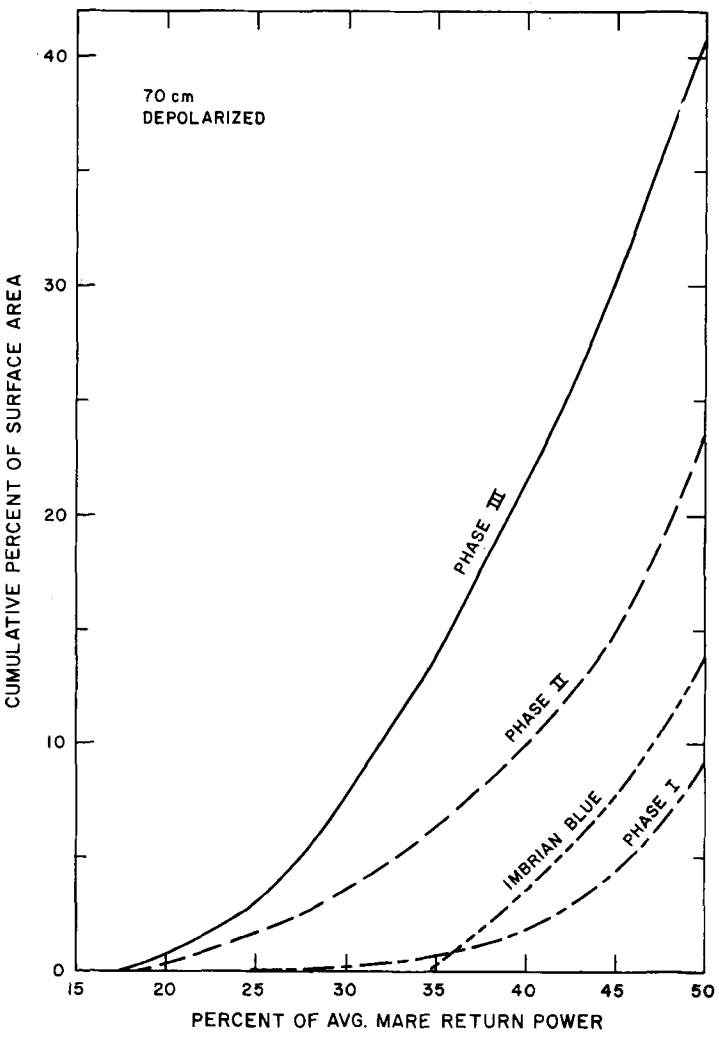

Fig. 8. Cumulative area percent of blue mare surfaces within Mare Imbrium characterized by less than 50 % of the average depolarized return for the basin. Surfaces represented shown in Figure 4.

We have shown that the blue mare surfaces within Mare Imbrium have a highly reduced depolarized radar return, especially at the 70 cm wavelength. If rock populations are the sole cause of depolarized radar variations, the inference is that abnormally low rock populations (>20 cm) characterize these surfaces. We will show that this is probably not the case.

Thompson *et al.* (1974) have suggested that increased lunar eclipse infrared temperatures associated with fresh impact craters are controlled by the abundance of surface rocks of greater than 10 cm diam; they further showed that photogeologic evidence and increased 3.8 cm and 70 cm radar backscatter data confirm this hypothesis. The inter-

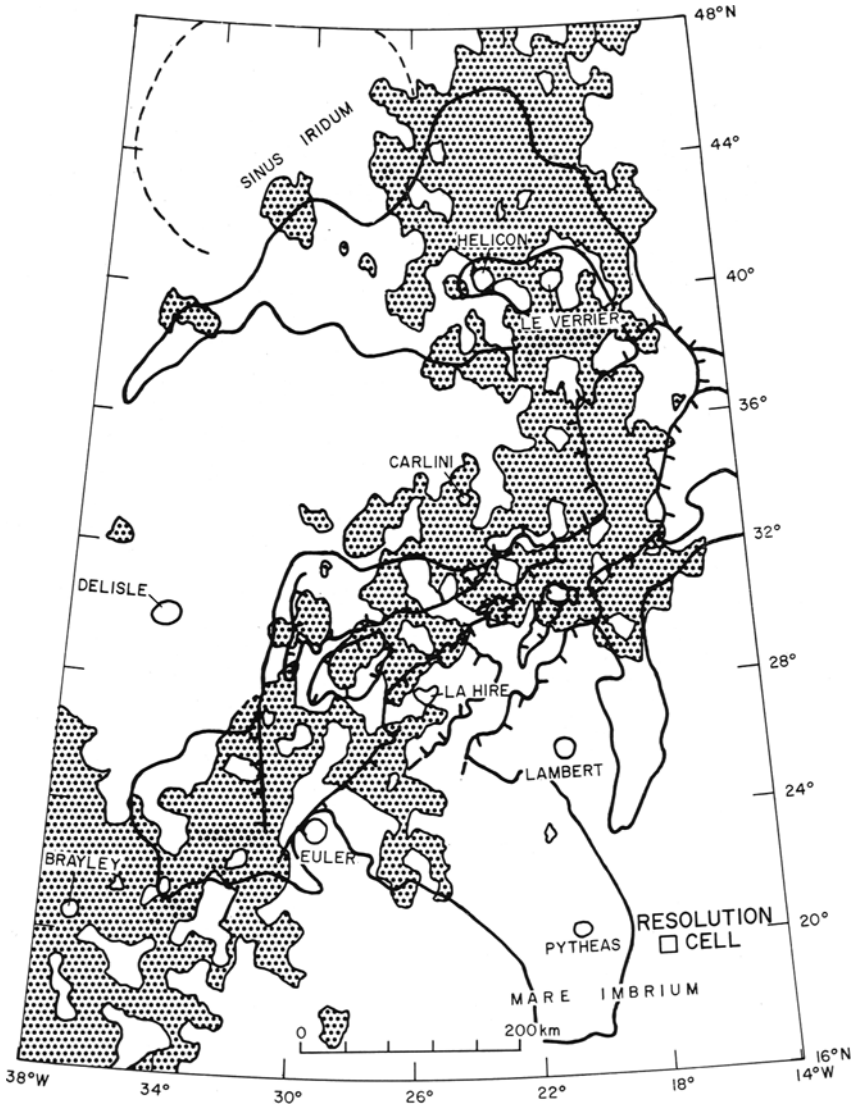

Fig. 9. Distribution of Mare Imbrium surface temperatures 5 K warmer than average for the basin; obtained from eclipse thermal (11 microns) data of Shorthill (1973). Eratosthenian mare surfaces described in Figure 1a. Thermal anomalies related to impact craters or ray material have been removed.

pretation of the regional variation in mare eclipse temperatures, however, is the subject of considerable debate (Hunt *et al.*, 1968; Buhl, 1971; Hagfors, 1970; Winter, 1970).

A modified 11 micron eclipse temperature image of the Imbrium basin shown in Figure 9 suggests that the Eratosthenian lava flows have slightly higher surface temperatures (5–10 K) than the older Imbrian materials. These data show the departures in temperature from an average temperature for the region (Shorthill, 1973).

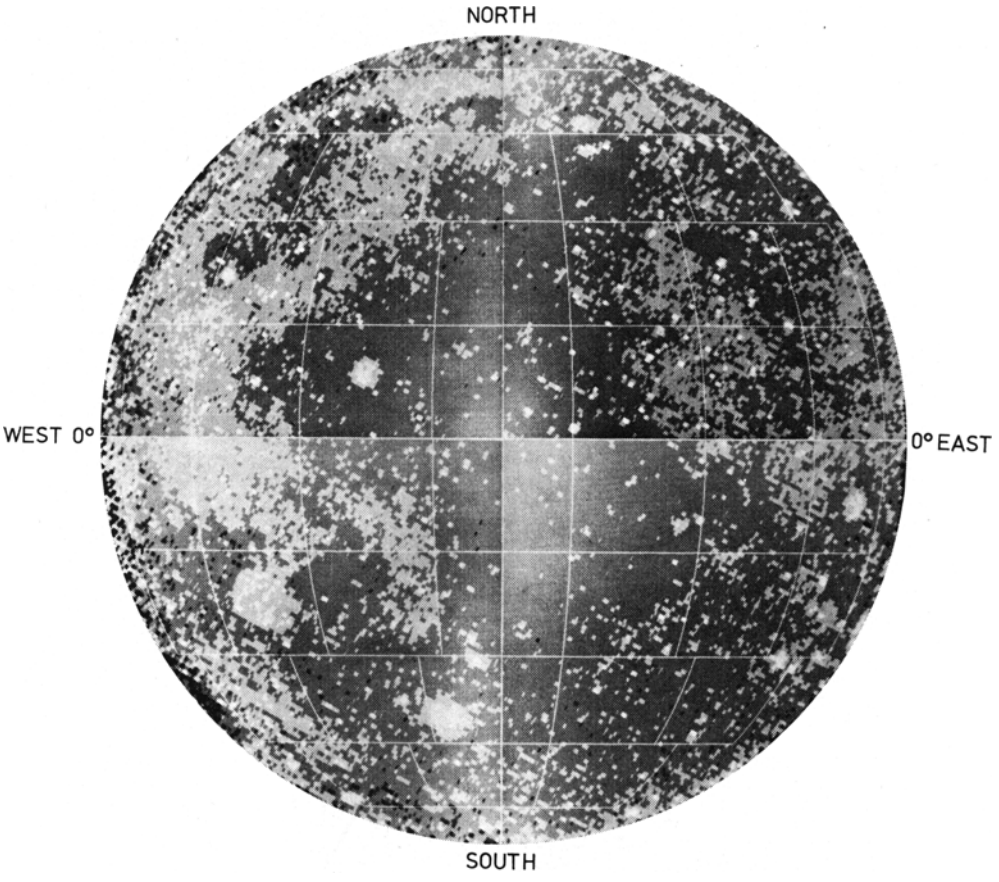

Fig. 10a. Infrared map of the Moon showing normalized eclipse temperatures, according to R. W. Shorthill and J. M. Saari. Lunar segments shown are LAC chart quadrangles shown on orthographic projection.

If increased rock populations are the cause of the regional mare eclipse temperature increases as previously suggested, then, what is the cause of the reduced radar backscatter? The major differences between the eastern and western lunar maria are the lower average albedo (Pohn *et al.*, 1970) and suspected higher titanium and iron content in the western hemisphere maria (Boyce *et al.*, 1974). One need only compare the eclipse IR data (Figure 10a) and the full Moon lunar albedo (Figure 10b) to observe a generally good correlation of low albedo and increased temperature within the lunar maria (Moore, 1974). It appears, then, that these two data sets are not reflecting the abundance of 10 cm and larger surface rocks but rather the distribution of surfaces with unusually low thermal inertias associated with lower visible albedo. On a local scale, of course, elevated thermal and albedo values can be related to the blocky ejecta and walls of large impact craters. Variations in lunar surface color have been shown to be intimately associated with changes in lunar albedo (low albedo,

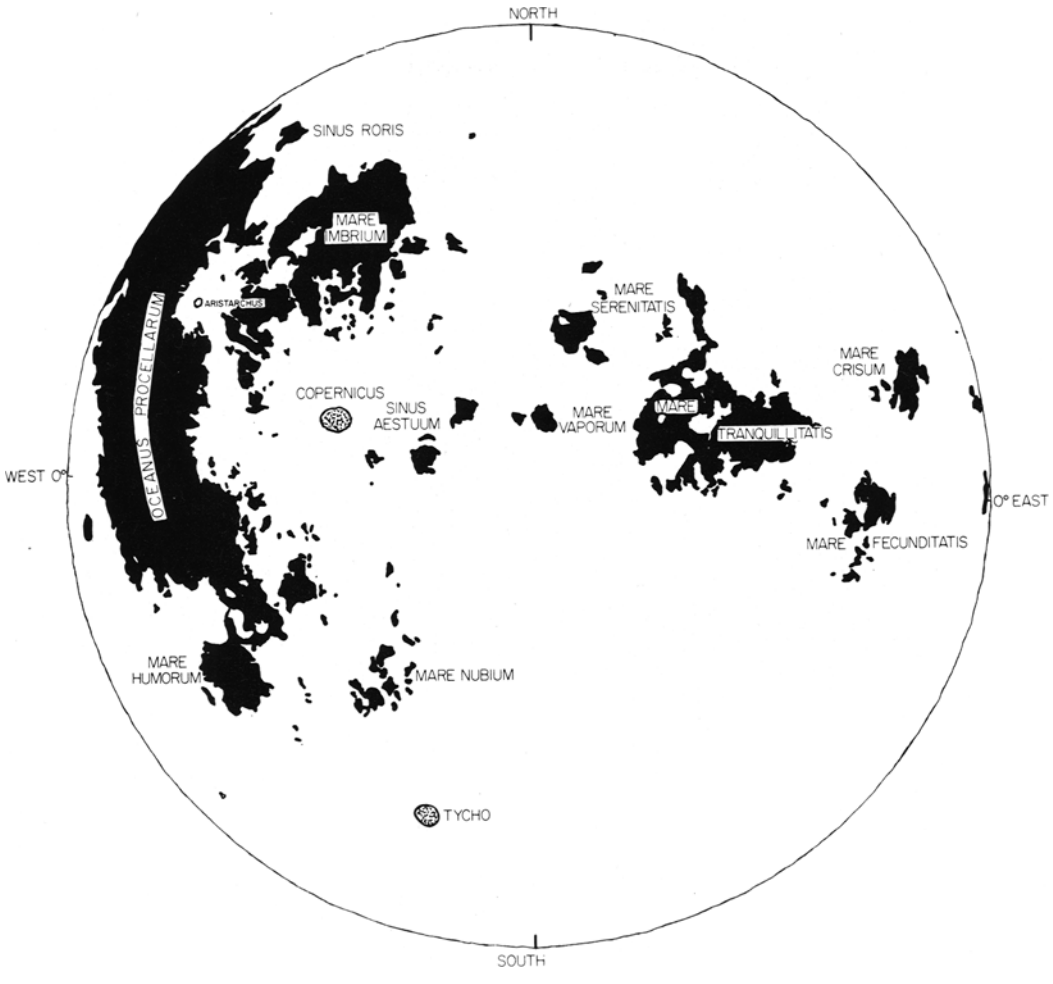

Fig. 10b. Distribution of lowest levels (0.074 to 0.090) of absolute visible albedo on the Lunar Earthside hemisphere (modified from Pohn *et al.*, 1970). Compare with elevated mare temperatures shown in Figures 9 and 10a).

blue color; high albedo, red color), both being related to chemical differences involving, primarily, titanium and iron.

5. Surface Slope Variations

Differences in root mean square (rms) surface slopes on the various mare units within Imbrium are not suspected as being a major factor in the observed radar behavior since the depolarized data from the blue surfaces reveal a sharp decrease in return power relative to the polarized return. The depolarized data, as stated earlier, contain primarily the diffuse component of the radar echo and little or no quasi-specular echo component expected from gentle surface undulations.

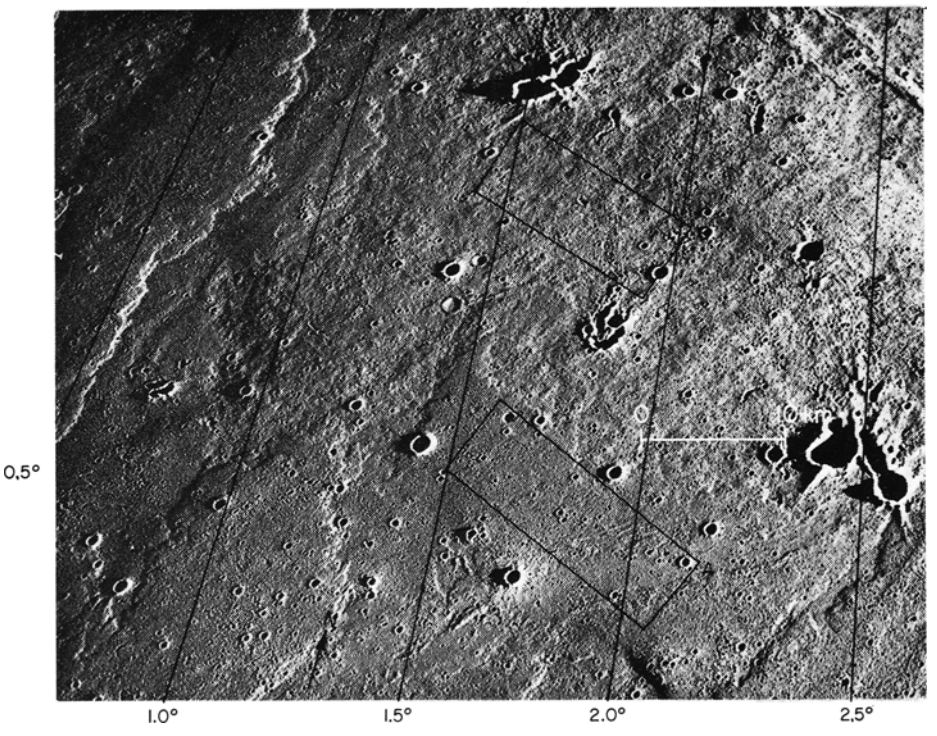

Fig. 11. Enlargement of Apollo 15 metric photograph (1557) showing phase III (A) and Imbrian blue (B) areas photometrically scanned for photoclinometric calculations of rms surface slopes. Number and lines represent Sun elevation angles in degrees. Area shown about 90 km west of La Hire (Figure 5a).

On low-sun Apollo photography, however, distinct kilometre-scale surface textural differences between the Imbrian blue and Eratosthenian phase III surface (Figure 11) can be observed. Utilizing the photoclinometric technique (Watson, 1968) we found the Imbrian blue area to have an average rms slope of 0.6 deg, the Eratosthenian phase III 0.4 deg, at a 3 km slope length scale.

Variations in surface slope at this scale are thought to be associated with smoothing of an underlying cratered surface by a younger eruptive sequence. Schaber *et al.* (1972) discussed the distinct association of flooded craters (1–4 km diam size) with weak radar return from the blue Eratosthenian surfaces in northern (phase I) and central (phase II) Imbrium. Further investigation of such flooded craters revealed that their numbers decrease with youth of the eruptive sequence, suggesting complete burial of all Imbrian and early Eratosthenian craters less than 4 km (diam) (150 m rim height) by the time of the phase III deposition.

We have at present no way of determining if the kilometre-scale surface-slope variations within Imbrium can be extrapolated down to the radar wavelength scales of 3.8 cm and 70 cm, but Surveyor and Apollo surface photography suggests little consistent textural difference below the metre scale for all visited mare sites that represent a 0.5 b.y.-range in age (including the Apollo 17 site).

6. Crater Size Frequency Distributions Within Imbrium

The crater size frequency distribution was determined for five mare surfaces within Imbrium (as shown in Figures 12a, b). Owing to the absence of high-resolution photography north of 32°N, only the phase III crater counts were extended down to the 25-m diam crater size. When the statistical error bars are considered, all blue surfaces (Imbrian blue and phases I, II, and III) are extremely close in >250-m diam crater populations. The old Imbrian red surface, characteristic of the eastern half of the basin, appears to be about two times more cratered than the average blue mare in the >250 m diam crater size range.

The frequency distribution of craters <150 m diam for the phase III flows is of special interest, since the number of craters decreases more rapidly than predicted by the steady state crater curve (Shoemaker *et al.*, 1968). These data are in agreement with recent findings of Howard *et al.* (1973) in Mare Serenitatis where the low albedo, blue, outer ring mare of that basin has been found to be older than the central red mare, contrary to pre-Apollo 17 concepts (Wilhelms and McCauley, 1971). The blue ring mare, though older, has fewer <150 m diam craters than the red central mare, and its crater-size frequency curve crosses that of the red at about the 150-m diam crater size (Wolfe, 1974).

There is then some evidence that the blue maria, on a lunar-wide scale, may have fewer craters of <150 m diam than red maria, regardless of their age relations. It appears, then, that poorly understood physical process, innate to the blue mare and dark mantled areas, preferentially destroys small craters on these surfaces much more rapidly than on the red mare surfaces. This parameter is being investigated at the Apollo 17 site where it may be caused by an anomalously thick unconsolidated layer (30 m; Wolfe (1974)) generated perhaps as a pyroclastic deposit and/or as a frothy upper-flow surface resulting from rapid degassing of a basalt liquid particularly high in titanium and volatiles.

7. Regolith Characteristics

There is some weak evidence suggesting that the regolith on the blue mare surfaces within Imbrium is anomalously thick as much as 2.5 times that expected by impact comminution of a coherent substrate. In Figure 13 increased depth of regolith is related to crater erosion ages for several Surveyor and Apollo landing sites utilizing the mare dating method of Soderblom and Lebofsky (1972)* and additional data from Boyce *et al.* (1974), Swann *et al.* (1972, 1975), Shoemaker *et al.* (1970a), and Moore (1974). Listed also on Figure 13 are the D_L values given by Schaber (1973) and

* The method involves visual examination of an orbital photograph to determine the maximum diameter of craters (D_s) whose internal slopes have been reduced to slopes less than the Sun elevation (S_s). Utilizing the Soderblom (1970) model of small-crater impact erosion, measurements of D_L are converted to an equivalent diameter (D_L) of a crater eroded to an interior slope of one degree under the same flux which has eroded a crater of diameter D_s to a slope of S_s. Values of D_L are considered synonymous with relative age which is directly proportional to the total number of craters that have accumulated on the surface.

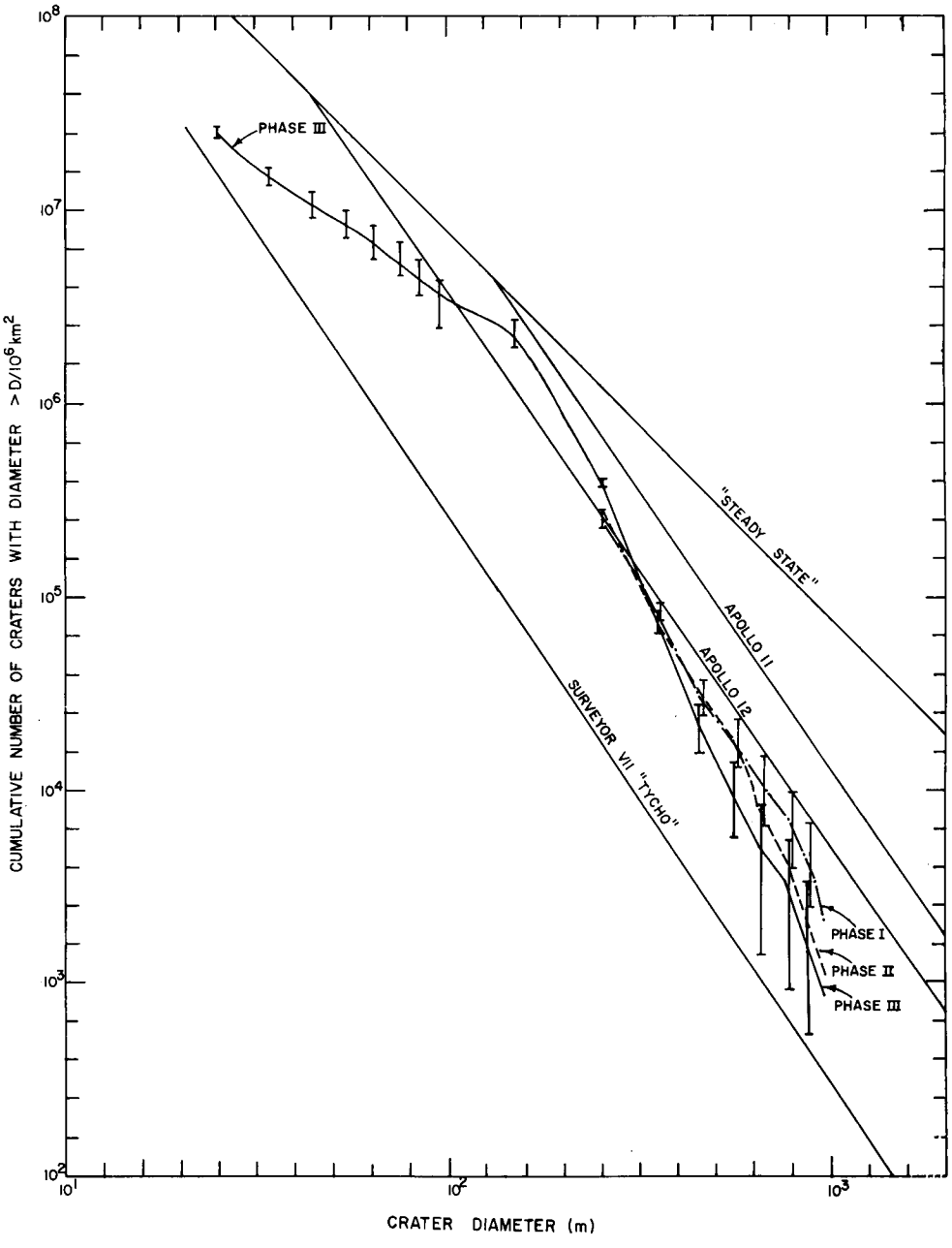

Fig. 12a. Crater-size frequency distribution for the Eratosthenian phase I, II, and III surfaces within Mare Imbrium. Phase III crater counts are extended down to 25 m diam owing to availability of high-resolution photography. The steady-state crater curve and the production crater curves of Apollos 11, 12, and Surveyor VII (Tycho crater rim) are shown.
Statistical error bars are included.

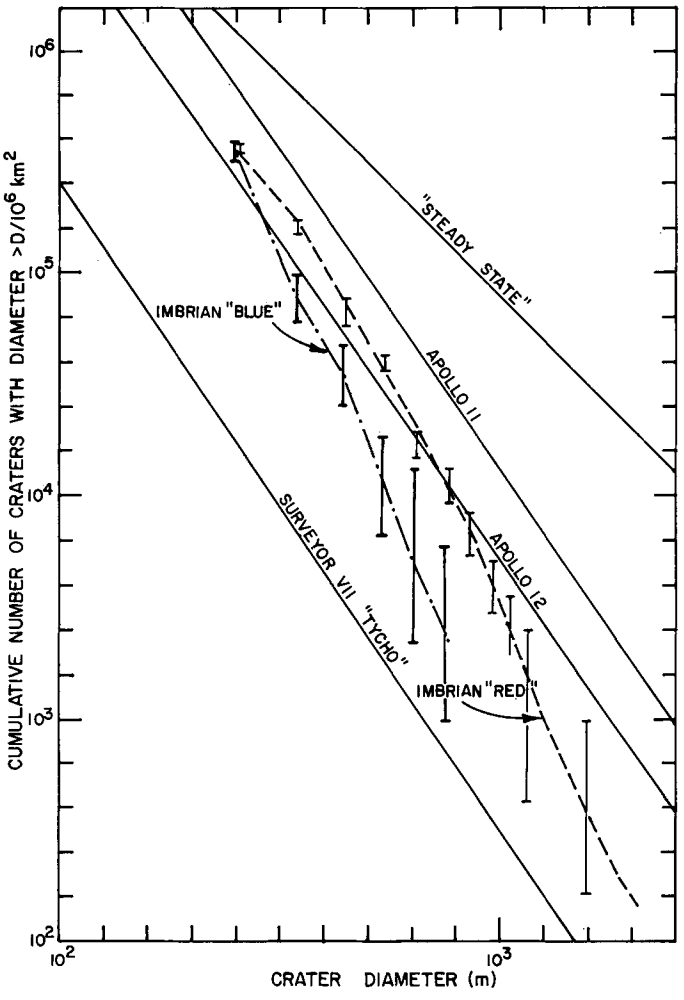

Fig. 12b. Crater-size frequency distribution for the Imbrian red and Imbrian blue surfaces within Mare Imbrium. See Figure 12a caption for explanation.

Boyce (1974) for various mare surfaces mapped within Imbrium. Note that for the latter, the predicted regolith depths vary from 5.2 m to 3.0 m, from oldest to youngest.

Oberbeck and Quaide (1968), using a statistical method based on small crater morphology, calculated an average 7.5 m regolith depth for a region (32° N, 22° W) including both an Imbrian blue and Eratosthenian phase III surface. This value is 1.9 to 2.5 times larger than the expected normal depths for these flow surfaces shown on Figure 13. The regolith thicknesses for these same two surfaces plus a phase II surface were rechecked utilizing the Oberbeck and Quaide method. Values of 5 m, 10 m, and 8 m were found for the Imbrian blue, phase II, and phase III surfaces, respectively, agreeing well with the earlier Oberbeck and Quaide data (Walker, 1974). The critical point is that at least the youngest blue lava surfaces within the Imbrium

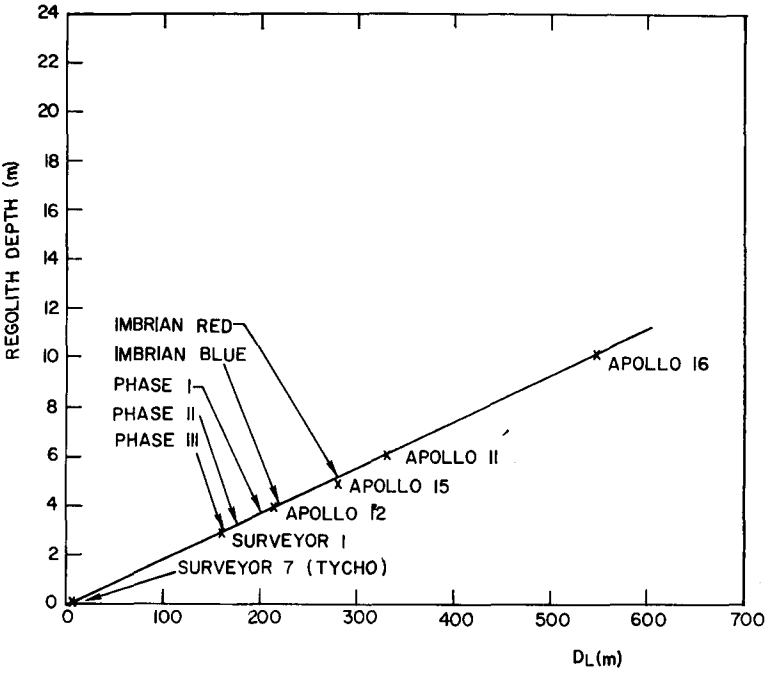

Fig. 13. Apparent regolith depths related to the surface crater erosion model age (D_L) of various Surveyor and Apollo sites as described by Soderblom and Lebofsky (1972) and Boyce *et al.* (1974). See text for definition of D_L and a discussion of their method of mare surface-age dating. The Mare Imbrium flow surfaces discussed are indicated on the curve.

basin (phase II and phase III) may have slightly greater apparent regolith depths and weak radar return.

Fielder and Fielder (1971) supplied additional evidence for the presence of a more compressible, and possibly thicker, regolith on the northernmost terminus (32°N, 22°W) of the phase III lava flows.* They pointed out the existence of a unique type of double-rimmed or benched craters on the phase III flow using Lunar Orbiter V high-resolution photography (frames H-159 and H-160). The benched craters on the phase III surface have a conspicuous deep pit in their floor whereas those on the underlying Imbrian blue surface are characterized by a flat, rubbly floor. There are virtually none of the deep pit type on the older surface and none vice versa. The presence on the young flow of the benched craters with the deep pit was attributed by Fielder and Fielder as evidence of a more compressible, frothy upper surface on the younger surface related to an abnormally rapid outgassing. We agree with this hypothesis.

It is difficult to accept the possibility that slight variations in regolith depth, rock populations, or small-crater frequencies on the blue Imbrium flows may be solely responsible for the rather large variations in radar attenuation demonstrated from

* Fielder and Fielder (1971) used the notations f1 and f3 for the Imbrian blue and phase III flows, respectively.

these surfaces. This is especially true as the radar attenuation is definitely unrelated to surface age when looked at on a lunarwide scale. Even within Imbrium, the older Imbrian blue surface has a greater attenuation in depolarized power than the younger Eratosthenian phase I surface (Table I).

The correlation of anomalous regolith thickness, weak radar reflectivity, and blue color appear to be the result of a 'fundamental' difference between the blue and red maria, their initial basalt chemistry. The chemistry, including the volatiles, affects the mode of deposition (Schaber, 1973) and is perhaps related to the rate of basalt extrusion as discussed by Nisbet and Pearce (1973) for terrestrial oceanic basalts.

8. Mare Color, Basalt Chemistry, and Radar Absorption Theory

We have shown that strongly reduced backscatter on both the 3.8 cm and 70 cm radar maps is associated with blue mare materials of Imbrian and Eratosthenian ages within the Imbrium basin. The most important physical differences between visible and radar enhanced 'scattering' are the effective penetration depth and the reflectivity which is a function of the size of surface scatterers. Both of these are related to the wavelength and have been described by classical laws of optics. It is the attenuation by absorption of these visible and radar signals that is critical to the present discussion. The physical mechanism generally given for the color absorption variations involves transfer of electronic charge involving Ti^{3+}, Ti^{4+} and Fe^{2+} ions in the glassy material of the agglutinates and the glasses of mare regolith (Adams and McCord, 1970; Conel and Nash, 1970; Charette *et al.*, 1974). Adams and McCord (1973) have recently considered additional reasons for the increased optical absorption by the glassy agglutinates to include (1) the presence of abundant finely disseminated metallic iron and other opaque phases (ilmenite most abundant) and (2) the abundance of microvesicles.

The physical mechanism responsible for radar absorption is less well understood than absorption in the visible spectrum. The degree of radar absorption by a material is a complex function given (Campbell and Ulrich, 1969) as the product of magnetic permeability and dielectric constant, and the sum of the loss tangents of the material. These parameters, in turn, are effected by permittivity, density of the material, temperature of the surface layers and macroscopic conductivity of intergrain boundaries within the material. These physical and electrical parameters are discussed within the lunar context in papers by Campbell and Ulrich (1969),Pollack and Whitehill (1972), and Alvarez (1974).

In the present discussion we have tried to characterize the results of radar behavior by showing a distinct correlation between increased absorption, blue color data, and mare stratigraphy. The positive correlation of these data sets strengthens the theory that some parameter (or parameters) related to basalt chemistry is responsible for the radar behavior in the maria. On a lunarwide scale, the depolarized return from the balsatic mare areas is consistently lower than that of the gabbroic-anorthosite highlands by a factor of between 2 and 5 at the 70 cm wavelength (Thompson, 1974).

Similar results have been reported for wavelengths ranging from 0.86 cm to 7.0 m (McCue and Crocker, 1972; Thompson, 1971).

Pollack and Whitehill (1972), in developing a physical model of lunar radar multiple-scattering suggested that the most important factor affecting the mare-highlands radar backscatter differences may be the radar absorption length in rocks and soil within the two regions – possibly related to ilmenite content. The absorption length of a material is defined as the distance over which an electromagnetic wave must travel in the material before being attenuated to $1/e$ (36.8%) of its initial intensity. Pollack and Whitehill (1972) suggest that a change in the absorption length of a factor of only 3.5 would be required to produce a change of a factor of 5 in the depolarized lunar radar return observed between the maria and highland. Campbell and Ultich (1969) reported absorption lengths of 7 m and 65 m in tholeiitic basalt and anorthosite powders (density = 1.0 g cm^{-3}), respectively, at the 70 cm (450 MHz) wavelength. They also reported absorption lengths of 0.4 m and 6.0 m in tholeiitic basalt and anorthosite solid rock at the 70 cm wavelength. The magnetic losses that may arise from the excessive ilmenite content in mare basalts (25% in Apollo 17 basalts) may be a significant factor in further reducing the absorption lengths in mare materials.

A primary question is whether the 70 cm radar signals are reaching through the mare regolith into the fractured substrate basalts, and if they are, where is the major absorption taking place? The absorption data of Campbell and Ulrich given above indicate that both the mare regolith and mare basalts could be highly attenuating to the signal. The 70 cm signals may be penetrating the highly absorbing mare regolith and encountering even greater attenuation in the highly titaniferous basaltic substrate.

Recent electrical properties measurements on returned Apollos 14, 16 and 17 samples by Sill (1974) have shown that the Apollo 17 (8–10% TiO_2) soils have significantly higher density (1.3 times), dielectric constant (1.3 times), and loss tangent (3.3 times) than those of Apollo 14 (2.0% TiO_2) and 16 (1.0% TiO_2) at a frequency of 10 Mhz. These values appear to be increasing directly with the titanium content, with the loss tangent showing the largest and perhaps the most significant variation with regard to signal absorption. The effect of increased dielectric constant or increased density alone would be to enhance the radar backscatter from regolith surfaces – the opposite of the observed behavior.

Additional laboratory radar research will be needed before the radar absorption phenomena can be fully understood. Special attention should be placed in the electrocal and magnetic effects of opaque minerals in glassy soils and basalts of the lunar type.

9. Calibration of TiO_2 and Radar Return

Charette *et al.* (1974) gave percent TiO_2 in bulk soils for 13 lunar regions obtained by calibration of slopes of spectral reflectivity curves utilizing return lunar sample spectral data. Included in the telescopically obtained spectral data were two regions within Mare Imbrium, one in the red Imbrian mare at the northeasteren edge of the (47°10′N; 9°50′W), the other in the phase I Eratosthenian blue mare near the crater

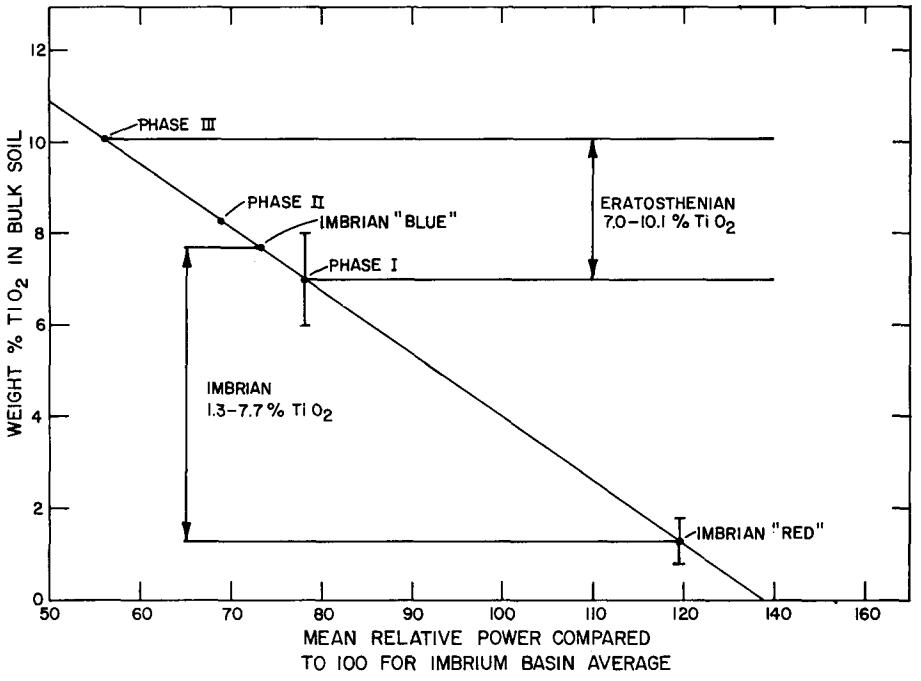

Fig. 14. Preliminary attempt at relating TiO_2 content in bulk regolith soils to a mean 70 cm depolarized return power for the five Imbrian and Eratosthenian study areas within Mare Imbrium. Mean return power for basin given as 100. Calibration of TiO_2 values limited to Phase I and Imbrian red surfaces after data given by Charette *et al.* (1974)

Helicon (38°45′N; 22°40′W) (Figure 1). These workers obtained a low value of $1.3 \pm .5\%$ TiO_2 for the red Imbrian age mare and a high 6–8 % for the blue phase I mare.

Utilizing these two data points within the basin and assuming a linear relation between TiO_2 content and average backscatter power from our frequency distribution data (Figures 7a, b, c), we have established a preliminary calibration curve to estimate TiO_2 content in Mare Imbrium bulk soils (Figure 14). The critical observation from this preliminary curve is that Imbrian surfaces within the basin appear to contain from 1 to 8% TiO_2 in bulk surface soils, whereas the Eratosthenian surfaces may vary from 7 to 10%. The Apollo 17 soils contain 10% TiO_2 (LSPET, 1973).

The authors are in the process of acquiring additional spectral reflectivity measurements within the Imbrium basin from which we can refine the calibration curve. Continuing research will also include calibration of the radar return from Apollo and Luna landing sites where physical, chemical and electrical data are available on the samples. The present lunar radar research should prove a powerful tool for lunar geochemical and geologic mapping and may be of significant value during preliminary analysis on available doppler-delay radar maps of Venus.

10. Conclusions

The present investigation has utilized geologic, photometric, colorimetric, and radar backscatter maps of Mare Imbrium to suggest a distinct association between individual basalt flows having blue color and greatly attenuated radar return. The main conclusions can be summarized as follows:

(1) Earth-based 3.8-cm and 70-cm polarized and depolarized radar return from Mare Imbrium decreases in average intensity from the older red to younger blue Imbrian surfaces and decreases from the oldest to youngest Eratosthenian surfaces, all of the blue spectral type.

(2) This reduced radar backscatter from the red to the blue mare surfaces is attributed to increased radar absorption in the blue, resulting, at least indirectly, from increased titanium and/or iron content in the basalts and overlying regolith. The important physical/chemical parameter may be increased concentrations of disseminated ilmenite opaques in a slightly deeper than normal glassy regolith.

(3) Titanium calibration of Earth-based radar backscatter maps is expected to provide a powerful new tool for lunar geochemical and geologic mapping as well as a means for preliminary geologic and geochemical analysis of Earth-based Venus radar backscatter maps.

Acknowledgements

Research sponsored by the National Aeronautics and Space Administration under a cooperative program involving Apollo experiments S-217 and S-222. Funding for U.S. Geological Survey by S-222 while support for the Jet Propulsion Laboratory is from S-217 and contract NAS7-100. Massachusetts Institute of Technology work supported under S-217.

Radar and infrared data displays and analyses were performed at the Image Processing Laboratory of the Jet Propulsion Laboratory (California Institute of Technology) and at the Haystack Observatory (Massachusetts Institute of Technology).

The authors thank Lyman Lyon (Jet Propulsion Laboratory) for radar display programming and the scientific illustration group of the U.S. Geological Survey (Flagstaff, Arizona) for their fine support.

References

Adams, J. B. and McCord, T. B.: 1970, *Proc. Apollo 11 Lunar Sci. Conf., Geochim. Cosmochim. Acta, Suppl.* 0, **3**, 1937–1945.

Adams, J. B. and McCord, T. B.: 1973, Mass. Inst. Tech. Planetary Astronomy Lab., Pub. No. 78, 35 p.

Boyce, J. M.: 1974, personal communication.

Boyce, J. M., Dial, A. L., and Soderblom, L. A.: 1974, *Proc. Fifth Lunar Sci. Conf., Geochim. Cosmochim. Acta, Suppl. 5*, in press.

Brown, W. E., Jr.: 1960, *J. Geophys. Res.* **65** (10), 3087–3095.

Buhl, D.: 1971, *J. Geophys. Res.* **76** (14), 3384–3390.

Burns, A. A.: 1969, *J. Geophys. Res.* **74** (27), 6553–6566.

Campbell, M. J. and Ulrich, J.: 1969, *J. Geophys. Res.* **74** (25), 5867–5881.

Charette, M. P., McCord, T. B., Pieters, C., and Adams, J. B.: 1974, *J. Geophys. Res.* **79** (11), 1605–1613.
Conel, J. E. and Nash, D. B.: 1970, *Proc. Apollo 11 Lunar Sci. Conf., Geochim. Cosmochim. Acta., Suppl. 1*, **3**, 2013–2023.
Fielder, G. and Fielder, J.: 1971, in G. Fielder (ed.), *Geology and Physics of the Moon*, Elsevier, pp. 15–26.
Hagfors, T.: 1967, *Radio Sci.* **2** (5), (new series), 445–465.
Hagfors, T.: 1970, *Radio Sci.* **5** (2), 189–227.
Howard, K. A., Carr, M. H., and Muehlberger, W. F.: 1973, *Apollo 17 Preliminary Science Report*, NASA SP-330, National Aeronautics and Space Administration; p. 29-1 to 29-12.
Hunt, G. R., Salisbury, J. W., and Vincent, R. K.: 1968, *Science* **162**, 252–254.
Kuiper, G. P.: 1965, Jet Propulsion Lab. Tech. Rept. 32-700, 9–73.
Lunar Sample Preliminary Examination Team: 1973, *Apollo 17 Preliminary Science Report*, NASA SP-330, National Aeronautics and Space Administration, p. 7-1 to 7-46.
McCue, J. J. and Crocker, E. A.: 1972, *J. Geophys. Res.* **77** (22), 4069–4078.
Moore, H. J.: 1974, unpublished data.
Nisbet, E. and Pearce, J. A.: 1973, *Nature* **246**, 468–470.
Oberbeck, V. R. and Quaide, W. L.: 1968, *Icarus* **9**, 446–465.
Pettengill, G. H. and Thompson, T. W.: 1968, *Icarus* **8** (3), 457–471.
Pettengill, G. H., Zisk, S. H., and Thompson, T. W.: 1974, *The Moon* **10**, 3–16.
Pieters, C., McCord, T. B., Adams, J. B., and Zisk, S. H.: 1973, *J. Geophys. Res.* **78** (26), 5867–5875.
Pohn, H. A., Wildey, R. L., and Sutton, G. E.: 1970, U.S. Geol. Survey Prof. Paper 599-E: U.S. Government Printing Office, Washington, D.C., 20 p.
Pollack, J. B. and Whitehill, L.: 1972, *J. Geophys. Res.* **77** (23), 4289–4303.
Rea, D. G., Heterington, N., and Mifflin, R.: 1964, U.S. Geol. Survey Misc. Map Series, I-602.
Schaber, G. G.: 1973a, *Apollo 17 Preliminary Science Report*, NASA SP-330, National Aeronautics and Space Administration, 30-17 to 30-25.
Schaber, G. G.: 1973b, *Proc. Fourth Lunar Sci. Conf., Geochim. Cosmochim. Acta, Suppl. 4*, 73–94.
Schaber, G. G., Thompson, T. W., and Eggleton, R. E.: 1972, *Nature* **226**, 1236–1239.
Shoemaker, E. M., *et al.*: 1968, Jet Propulsion Lab. Tech. Rept. 32-1265, 21-136.
Shoemaker, E. M., *et al.*: 1970a, *Science* **167**, 3918, 452–455.
Shoemaker, E. M., *et al.*: 1970b, *Apollo 12 Preliminary Science Report*, NASA SP-235, National Aeronautics and Space Administration, 113–156.
Shorthill, R. W.: 1973, *The Moon* **7** (1/2), 22–45.
Sill, W. R.: 1974, personal communication.
Soderblom, L. A.: 1970, *J. Geophys. Res.* **75** (14), 2655–2661.
Soderblom, L. A. and Lebofsky, L. A.: 1972, *J. Geophys. Res.* **77**, 279–296.
Swann, G. A., *et al.*: 1972, *Apollo 15 Preliminary Sci. Rep.* NASA SP-289, National Aeronautics and Space Administration, 5-1 to 5-112.
Swann, G. A., *et al.*: 1975, U.S. Geol. Survey Prof. Paper 880 (in press).
Thompson, T. W.: 1971, *Icarus* **13**, 363–370.
Thompson, T. W.: 1973, *Apollo 17 Preliminary Science Report*, NASA SP-330, National Aeronautics and Space Administration 33-3 to 33-10.
Thompson, T. W.: 1974, *The Moon* **10**, 51–85.
Thompson, T. W. and Zisk, S. H.: 1972, Progress in Aeronautics and Astronautics, M.I.T. Press, Cambridge, Mass., 83–117.
Thompson, T. W., Masursky, Harold, Shorthill, R. W., Tyler, G. L., and Zisk, S. H.: 1974, *The Moon* **10**, 87–117.
Walker, A.: 1974, personal communication.
Watson, Kenneth: 1968, U.S. Geol. Survey. Paper 599-B, 10 p.
Whitaker, E. A.: 1972, *The Moon* **4**, 348–355.
Whitaker, E. A.: 1974, personal communication of work in progress.
Wilhelms, D. E. and McCauley, J. F.: 1971, Geologic Map of the Near Side of the Moon, Geologic Atlas of the Moon, Near Side of the Moon I-703, U.S. Geol. Survey., Washington, D.C.
Winter, F.: 1970, *Radio Sci.* **5** (2), 229–240.
Wolfe, E. W.: 1974, peronal communication.
Zisk, S. H., Pettengill, G. H., and Catuna, G. W.: 1974, *The Moon* **10** (1), 17–50.